p-24 Measurement of substrate impurity fluctuation in CCD image sensors

Hiromitsu Shiraki, Takayuki Kimura, Takanori Arano, and Noboru Takatsuka
System Department, Faculty of Engineering, Ibaraki University

1. Introduction

The saturation signal level of a CCD image sensor with a vertical over-flow drain varies strongly with substrate impurity concentration. Therefore, substrate impurity concentration fluctuation appears as a fixed pattern noise for the saturation exposure. We have clarified the relationship between the saturation signal level and the substrate impurity concentration by using one-dimensional analysis. Then, we compared the relationship with that obtained by using three-dimensional numerical analysis in order to examine the effectiveness of the one-dimensional analysis. By comparing the results of the three-dimensional analysis with the saturation signals of CCD image sensors, the substrate impurity concentration fluctuation was determined. Moreover, specific features of impurity fluctuation in the wafers grown by various methods, permissible and measurable impurity fluctuation levels, and a photodiode structure that can suppress the saturation level fluctuation will be discussed.

2. One-Dimensional Analysis

Figure 1 shows an example of a photodiode structure and potential profiles along the depth (X) direction taking charge storage width (W) as a parameter. This structure is designed only for analysis, so it differs from an actual device structure. The overflow current density (J_{OF}) can be calculated from Fig. 1 as follows:

$$J_{OF}=-qD_nN_{ST}\exp(-qV_{BR}/kT)(1-\exp(qV_{CS}/kT)) / \int_{barrier}\exp(\Psi(X-X_F)/kT)dX. \quad 1$$

In equation 1, D_n: electron diffusion constant, N_{ST}: donor concentration in the storage layer, V_{BR}: barrier height, V_{CS}: Fermi level difference between charge storage region and substrate, and $\Psi(X-X_F)$: potential increase at X from the minimum potential at X_F. J_{OF}'s are shown in Fig. 2 as a function of W taking substrate impurity concentration as a parameter. It is seen from Fig. 2 that J_{OF} increases exponentially with W. In this case, effective photocurrent density J_{PH} that flows into the storage region can be expressed as follows,

$$J_{PH}=-qWN_{ST}/T_S \quad 2,$$

where T_S is the storage time. J_{PH} is also illustrated in Fig. 2 for T_S=82.3 ms that is used in the experiments described below. W's at the cross points of J_{PH} and J_{OF} are the saturation charge storage widths. W's are proportional to the

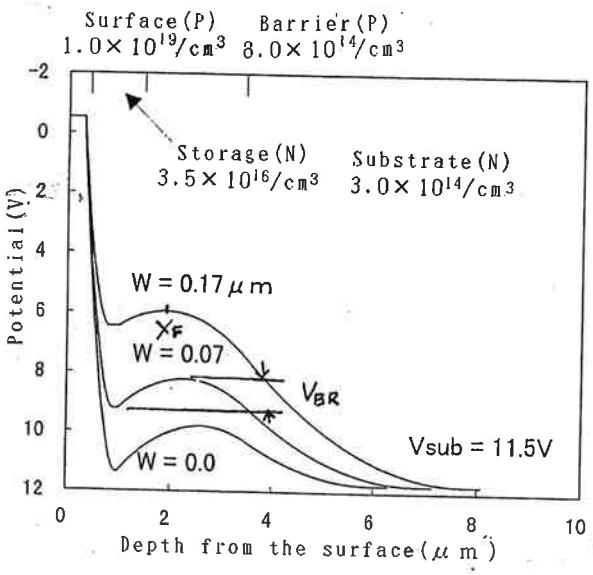

Fig. 1 Photodiode structure and potential profiles along the depth(x) direction.

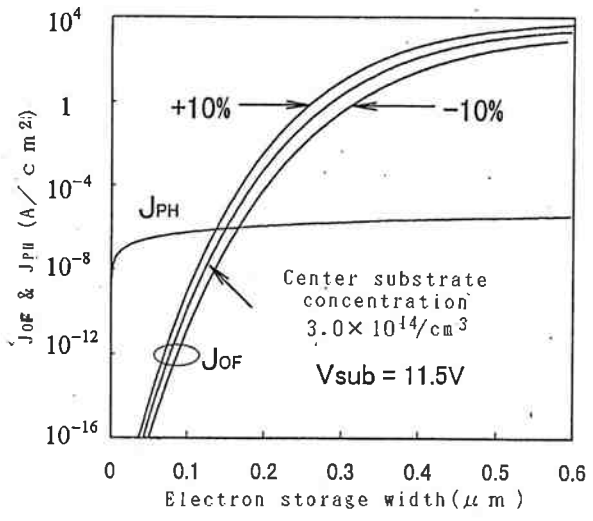

Fig. 2 Over-flow current and photocurrent density as a function of charge storage width

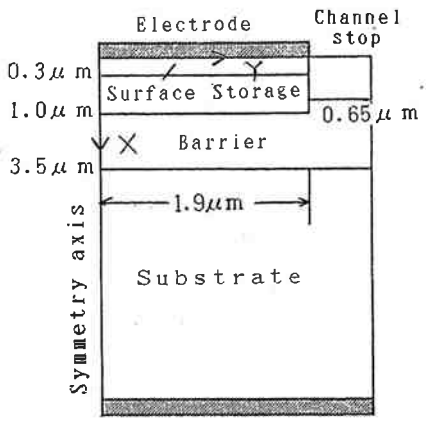

(a) Conventional channel stop,

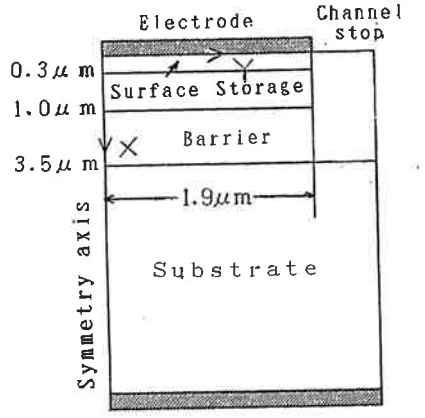

(b) Deep channel stop.

Fig. 3 Models of photodiode for three-dimensional analysis

saturation signal level. We can obtain substrate impurity concentration fluctuation by adapting Fig. 2 to saturation signal fluctuations if the central impurity concentration is known. It was also clarified that the saturation signal fluctuation becomes remarkable when the substrate voltage is increased. This result coincides with the experimental results.

3. Three-dimensional analysis

Figure 3(a) is a cross-sectional view of a photodiode used to simulate the saturated signal level by using three-dimensional analysis. Since a large percentage of an actual photodiode is generally surrounded by channel stop region, it will be reasonable to use the model shown above. The structure of the photodiode in the depth direction is same as that shown in Fig. 1. In the simulation, the number of electrons in the storage layer is set to zero at first, then irradiation which is strong enough to cause the signal level saturation, begins and continues during storage time (82.3 ms). The number of the stored electrons is counted at every one-tenth interval of the storage time. Table 1 shows the increase in the stored electrons, in the course of the storage, for different substrate impurity concentrations. We can see from the table that almost the same amount of electrons are stored in each photodiode before saturation. However a marked difference takes places at the saturation. These results agree qualitatively with the experimental results. The following conclusions were obtained from the comparison of the two analyses:

(1) The number of stored electrons increases (decreases) with a decrease (increase) of substrate impurity concentration for both analyses.

(2) The ratio of the increase (decrease) of the stored electrons calculated by the three-dimensional analysis to that by the one-dimensional analysis is a little smaller than unity.

This small discrepancy can be explained as follows: Namely, in the three-dimensional structure, the channel stop region lowers the barrier potential to weaken the effect of impurity fluctuation on the saturated level fluctuation. When one-dimensional analysis is adopted to calculate the impurity fluctuation, it gives a lower fluctuation value than the actual one. However one-dimensional analysis remains an easy way to determine the impurity fluctuation.

Figure 3(b) shows a new photodiode structure designed to minimize the effect of substrate impurity fluctuation at the saturation level. Figure 3(b) has deep channel stop region. In Fig. 3(b), the donor concentration in the barrier region and acceptor concentration are $4.5\times10^{16}/cm^3$ and $4.0\times10^{14}/cm^3$, respectively. The barrier width is 3.0 μm. The vertical impurity profile is similar to that of the measured device except for the step impurity profile. Again, three-dimensional analyses were carried out for a conventional photodiode structure with shallow channel stop region (Fig.3 (a)) that has a vertical impurity profile shown in Fig. 3(b) (PD1) and a photodiode directly shown in Fig. 3(b) (PD 2). In addition, one-dimensional analysis could not be applied to

Subst. con.	−10%	Center	+10%
	Stoted electron (×10⁵)		
0	0	0	0
S 2	.37	.36	.36
T 4	.71	.70	.53
E 6	.88	.86	..85
P 8	1.04	1.02	1.00
9	1.20	1.10	1.02
10	1.20	1.10	1.02

Table 1 Number of stored electrons during a storage time for different substrate impurity concentrations.

Structure	Fig.3(a) VSUB=11.5V			Fig.3(b) VSUB=25V		
Subst. con.	−10%	Center	+10%	−10%	Center	+10%
	Stored electron (×10⁵)			Stored electron (×10⁵)		
10	0	0	0	0	0	0
S 12	.31	.31	.31	.63	.62	.62
T 14	.60	.60	.59	1.23	1.22	1.22
E 16	.88	.87	.86	1.81	1.80	1.80
P 18	1.00	1.01	.98	2.35	2.33	2.32
19	1.06	1.02	.98	2.58	2.55	2.53
20	1.07	1.02	.98	2.58	2.56	2.53

Table 2 Number of stored electrons during a storage time for different photodiode structures and substrate impurity concentrations.

PD1 and PD2, because the barrier region became neutral when W increased. This is the reason why we used the vertical structure shown in Fig.1 to examine the accuracy of the one-dimensional analysis.

Table 2 shows the variations in the amount of stored electrons in PD1 and PD2, during charge storage period, for different substrate impurity concentrations. We can see from Table 2 that, in PD1, the amounts of stored electrons depend on the substrate impurity concentrations at only the saturation level. On the other hand, in PD2, the amounts of the stored electrons hardly depend on the substrate impurity concentration even at the saturation level. These results are due to the fact that since the barrier region potential in PD1 is severely lowered by the channel stop region potential, the substrate impurity fluctuation hardly modulates the minimum potential in the barrier region. Therefore, the amount of stored electrons is only slightly affected by the substrate impurity concentration. These situations are shown in Figs. 4(a) and (b). We can see the high and low barrier potentials in Fig. 4 (a) and Fig. 4 (b), respectively.

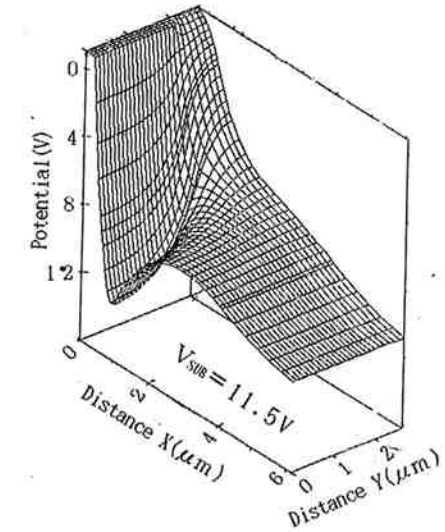

(a) Conventional channel stop.

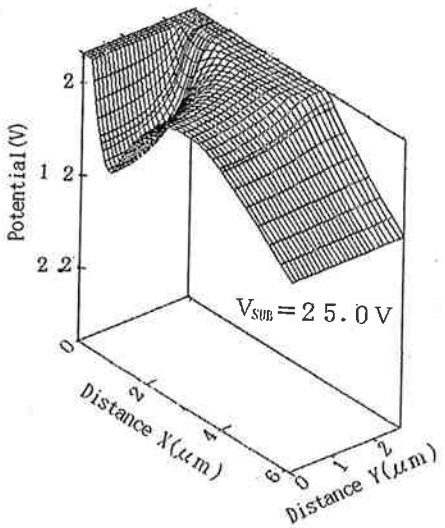

(b) Deep channel stop..

Fig. 4 Potential profiles at the beginning of charge storage.

4. Experimental results

A 320(H)×247(V)-pixels interline-scheme CCD image sensors were made on CZ, MCZ, and epitaxial wafers. The pixel pitch is 10-μm in both directions. Reproduced images at the saturation were taken to clarify the macroscopic substrate impurity fluctuation. Also, horizontal-line video signals were measured to determine the microscopic impurity fluctuation. Figure 5(a) shows a reproduced image obtained from a chip on the peripheral region of the CZ wafer. High substrate bias (11.5 volts) was used to obtain high image and signal contrast. Figure 5(b) shows a horizontal-line video signal corresponding to the central part of Fig. 5 (a). The saturation level fluctuation reaches

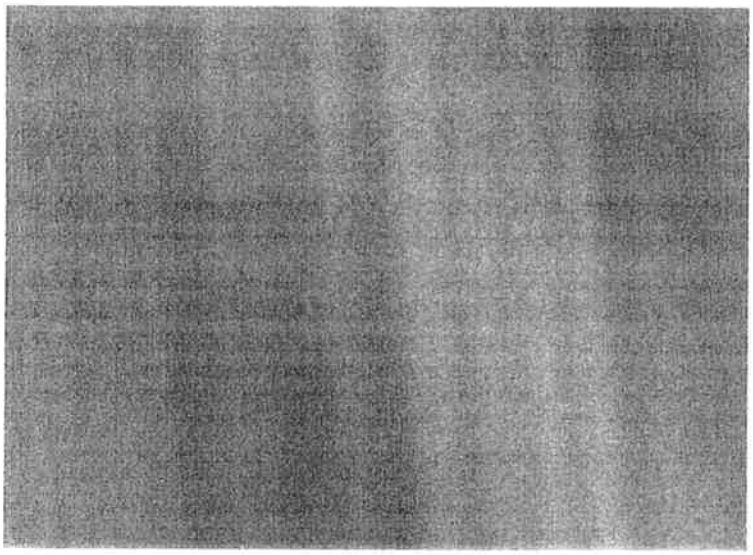

(a) Reproduced image at V_{SUB}=11.5 volts.

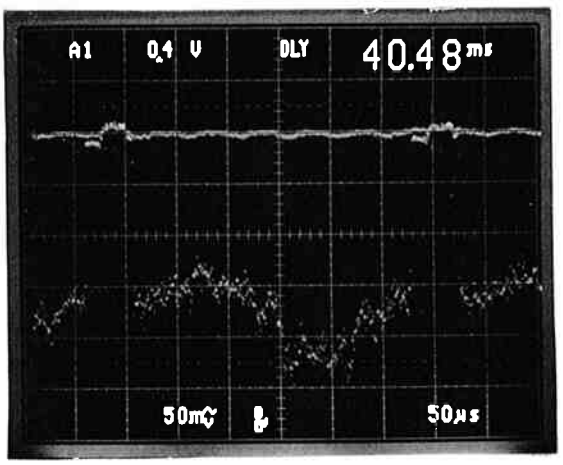

(b) A horizontal line signal.

Fig. 5 Reproduced image and its horizontal line signal.

to almost ±30%. By comparing Fig.5 (b) and the result of the three-dimensional analysis, it was clarified that impurity fluctuation reaches to ± 67.5%. This value is about 4 times larger than the generally believed. One reason for the very large impurity fluctuation is probably that the CCD chip is located at the peripheral region of a wafer with large impurity concentration fluctuation. The other reason is that since the sampling area for impurity fluctuation measurement is as small as the photo diode area (≒ 10 μ m^2), microscopic impurity fluctuation, that is averaged in the usual 4 points probe method, is detected. However it is important to use an exact impurity profile to obtain accurate substrate impurity fluctuation. Impurity fluctuations in the MCZ wafer were 1.5-times larger than in the CZ wafer at the peripheral region. In the central part of these wafers, the fluctuations decreased to 50% of the peripheral values. The fluctuation in the epitaxial wafer was almost 20-30% of the CZ wafer peripheral region. When the substrate bias is decreased to 6 volts, which is sufficient enough to suppress blooming, the saturation level fluctuation decreased to ±10%.

It is generally said that if fixed pattern noise is 40 dB's lower than the mean signal level, the human eye cannot recognize the noise. To achieve this condition, substrate impurity fluctuation must be lower than±0.55% at V_{SUB}=11.5 volts and ±1.5% at V_{SUB}=6.0 volts. This fluctuation level has not been attained even in epitaxial wafers. In fact, saturation level fluctuations were observed in epitaxial wafers at V_{SUB}=6 volts. The detectable impurity fluctuation is limited by the noise in CCD sensor. When taking reset noise and amplifier noise into consideration, substrate impurity fluctuation of less than ±0.1% will be detected at V_{SUB}=11.5 volts.

The swirl pattern in Fig.5 (a) includes a lot of black and white dots. These dots severely degrade the image quality. We are not sure if these dots are caused only from substrate impurity concentration fluctuation. Detailed impurity fluctuation analyses and lattice defect analyses will be needed to clarify the mechanism that generate these dots.

Acknowledgement

We would like to express their sincere thanks to the Foundation for Promotion of Material Science and Technology for funds at 1996 and 1998 and to The Ministry of Education, Science, Sports and Culture for Grant-in AID for Scientific Research (No.08455159) during 1996-1998.

〒316-8511 4-12-1 Naka-Narusawa, Hitachi City, Ibaraki Prefecture, Japan.
Fax & Tel. 0294-38-5187 e-mail shiraki@ipc.ibaraki.ac.jp